Estimation of the Variation in Specific Discharge Over Large Depth Using Distributed Temperature Sensing (DTS) Measurements of the Heat Pulse Response

des Tombe, Bas F.; Bakker, Mark; Smits, Frank; Schaars, Frans; van der Made, Kees Jan

DOI
10.1029/2018WR024171

Publication date
2019

Document Version
Final published version

Published in
Water Resources Research

Citation (APA)
des Tombe, B. F., Bakker, M., Smits, F., Schaars, F., & van der Made, K. J. (2019). Estimation of the Variation in Specific Discharge Over Large Depth Using Distributed Temperature Sensing (DTS) Measurements of the Heat Pulse Response. *Water Resources Research*, *55*(1), 811-826. https://doi.org/10.1029/2018WR024171

Water Resources Research

RESEARCH ARTICLE
10.1029/2018WR024171

Estimation of the Variation in Specific Discharge Over Large Depth Using Distributed Temperature Sensing (DTS) Measurements of the Heat Pulse Response

Bas F. des Tombe[1], Mark Bakker[1], Frank Smits[1,2], Frans Schaars[3], and Kees-Jan van der Made[4]

[1]Water Resources Section, Faculty of Civil Engineering and Geosciences, Delft University of Technology, Delft, Netherlands, [2]Waternet, Amsterdam, Netherlands, [3]Artesia, Schoonhoven, Netherlands, [4]Wiertsema & Partners, Tolbert, Netherlands

Key Points:
- A fiber-optic cable and a heating cable are inserted together using direct push
- The variation of groundwater flow perpendicular to the cables is estimated from a heat pulse response test
- Magnitude of the flow is determined without knowledge of the relative position of the two cables

Supporting Information:
- Supporting Information S1
- Data Set S1

Correspondence to:
B. F. des Tombe,
b.f.destombe@tudelft.nl

Citation:
des Tombe, B. F., Bakker, M., Smits, F., Schaars, F., & Van Der Made, K.-J. (2019). Estimation of the variation in specific discharge over large depth using Distributed Temperature Sensing (DTS) measurements of the heat pulse response. *Water Resources Research*, *55*. https://doi.org/10.1029/2018WR024171

Received 27 SEP 2018
Accepted 21 DEC 2018
Accepted article online 3 JAN 2019

Abstract An approach is presented to determine groundwater flow in unconsolidated aquifers with a heat pulse response test using a heating cable and a fiber-optic cable. The cables are installed together using direct push so that the cables are in direct contact with the aquifer. The temperature response is measured for multiple days along the fiber-optic cable with Distributed Temperature Sensing (DTS). The new approach fits a two-dimensional analytical solution to the temperature measurements, so that the specific discharge can be estimated without knowledge of the position of the fiber-optic cable relative to the heating cable. Two case studies are presented. The first case study is at a managed aquifer recharge system where fiber-optic cables are inserted 15 m deep at various locations to test the fitting procedure. Similar and relatively large specific discharges are found at the different locations with little vertical variation (0.4–0.6 m/day). The second case study is at a polder, where the water level is maintained 2 m below the surrounding lakes, resulting in significant groundwater flow. The heating and fiber-optic cables are inserted to a depth of 45 m. The specific discharge varies 0.07–0.1 m/day and is significantly larger in a thin layer at 30-m depth. It is shown with numerical experiments that the estimated specific discharge is smoother than in reality due to vertical conduction, but the peak specific discharge is estimated correctly for layers thicker than ~1.5 m.

1. Introduction

The calibration of groundwater models requires measurements of both head and flow. While head can be measured directly, flow can only be measured either when it enters or exits the aquifer (e.g., wells, seepage meters, and river discharge), or indirectly with tracers (e.g., solutes and heat) or a variety of geophysical techniques. In this paper, the specific discharge is estimated from a heat pulse response test using a heating cable and a fiber-optic cable that are installed together with direct-push equipment to a depth of tens of meters. The temperature response is measured along the fiber-optic cable with Distributed Temperature Sensing (DTS) from which the specific discharge is estimated without knowledge of the position of the fiber-optic cable relative to the heating cable.

The use of heat as a tracer has increased over the past decades (e.g., Anderson, 2005; Saar, 2011). Pioneering work on the use of heat as a tracer started in the 1960s with determining groundwater recharge from annual temperature fluctuations at the surface (Bredehoeft & Papadopulos, 1965; Stallman, 1965; Suzuki, 1960), which was extended to the basin scale by Cartwright (1970) and Domenico and Palciauskas (1973). Somogyvári and Bayer (2017) applied inversion algorithms from seismic tomography to a thermal tracer test to reveal aquifer features between two shallow wells. In the 1990s probes were developed with a needle-like heater and thermocouple to determine thermal properties of soil samples (e.g., Ren et al., 1999). Later on, these probes were used to estimate groundwater flow (e.g., Banks et al., 2018; Greswell et al., 2009; Ren et al., 2000). The exact distance between the heater and thermocouple proved to be a large source for errors (Greswell et al., 2009; Kluitenberg et al., 1995), which limits its practical use to small scale measurements. Thermal response tests were also used in other fields, for example, to measure wind speeds (Sayde et al., 2015).

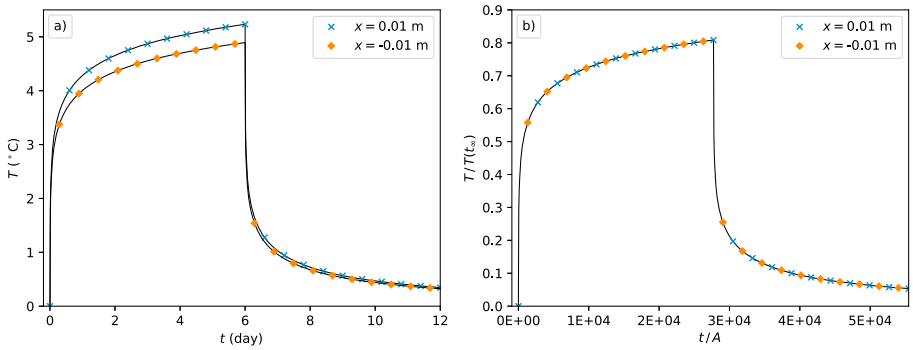

Figure 1. (a) Example of a temperature response 1 cm downstream (blue crosses) and 1 cm upstream (orange diamonds) of the heat source using the mean parameter values in Table 2 and $q = 0.5$ m/day. (b) Nondimensionalized form of the temperature response shown in Figure 1a.

Groundwater flow can also be estimated from characteristic thermal signatures on a borehole temperature log using naturally occurring temperature gradients (e.g., Drury et al., 1984; Reiter, 2001; Trainer, 1968). The use of DTS adds great detail to thermal response measurements in boreholes; a review of several applications is given in Bense et al. (2016). Layering of the subsurface can be characterized when the borehole is heated (e.g., Leaf et al., 2012). Fractures in bedrock can be identified by temporary sealing parts of the borehole (e.g., Coleman et al., 2015). Read et al. (2014) actively heated a fiber-optic cable to estimate the vertical flow in a well. Thermal response tests are also regularly applied in the field of geothermal energy to quantify the horizontal groundwater flow, which significantly affects the performance of geothermal systems (Chiasson et al., 2000). The performance of ground-coupled heat pumps can be assessed in aquifers with significant groundwater flow by idealizing the borehole as infinitely thin and neglecting vertical heat transfer (e.g., Diao et al., 2004; Wagner et al., 2013, 2014). The findings of Diao et al. (2004) were used by Selker and Selker (2018), who presented a method to estimate the vertical variation in the horizontal specific discharge from the thermal response measured in a grouted borehole.

The use of a heating cable in a borehole introduces four additional challenges when estimating groundwater flow. First, large temperature gradients in a borehole may result in vertical flow in the borehole (e.g., Drury et al., 1984). Second, permeable layers are cross-connected vertically via open boreholes and filter beds (e.g., Coleman et al., 2015; Pehme et al., 2007, 2010). Third, the filter and the filter pack affect the horizontal streamlines (Drost et al., 1968). Fourth, the exact positions of the heating cable and temperature sensors in the borehole are difficult to determine at depth, while they greatly influence the estimates of the thermal properties (Moscoso Lembcke et al., 2015).

The use of boreholes may be avoided in unconsolidated aquifers by installing fiber-optic and heating cables with direct push (Bakker et al., 2015), where it is assumed that the installation does not disturb the flow field. A thermal response can be measured accurately along the fiber-optic cables with DTS. Bakker et al. (2015) performed two tests in relatively homogeneous dune sand of a managed aquifer recharge system where the specific discharge was relatively large (0.5 m/day). In the first test, the magnitude of the specific discharge was determined up to 20-m depth from a heat pulse response test where a heating cable and a fiber-optic cable were installed together. The heating and fiber-optic cables were taped together, but they twisted around each other during installation. As a result, the position of the fiber-optic cable relative to the heating cable in the subsurface was unknown, which significantly affected the measured temperature increase during heating, even when the centers of the two cables were just 1 cm apart (see Figure 1a). As a result, only the measured temperature decrease during cooling (after the heating cable is turned off) was used to determine the specific discharge. In the second test, Bakker et al. (2015) determined both the magnitude and the direction of the specific discharge from five additional fiber-optic cables that were installed around the heating cable at distances of 1–2 m. The exact positions of the fiber-optic cables relative to the heating cable were known at the surface, but unknown at depth as installation of the cables with direct push gives small deviations from the vertical that were not measured.

The objective of this paper is to determine the magnitude of the specific discharge from a heat pulse response test with one heating cable and one fiber-optic cable, like the first test in Bakker et al. (2015). First, a new

approach is presented to determine the specific discharge from the temperature measurements during both heating and cooling when the position of the fiber-optic cable relative to the heating cable is unknown. This approach is tested in Case Study I, which uses the data of the heat pulse response test presented in Bakker et al. (2015). The range of applicability of the approach was explored by carrying out Case Study II, where the fiber-optic and heating cables were installed much deeper (up to 45 m) and the specific discharge was much smaller and was expected to have a larger variation with depth. Finally, three aspects affecting the accuracy of the proposed method on the estimated specific discharge are explored: vertical conductive heat transfer, hydrodynamic dispersion, and heterogeneity in horizontal layers.

2. Mathematical Formulation

Consider combined groundwater flow and heat transfer in a horizontally infinite aquifer. The aquifer is discretized vertically in many horizontal layers. Water and heat are approximated to move only within a layer; vertical transfer between layers is neglected (but is considered in section 6). Each layer is homogeneous, with a steady state uniform groundwater flow aligned with the x axis. Viscosity and density effects, if any, are neglected. The temperature of both the water and the solids is approximated to be at instantaneous equilibrium. The temperature distribution in a layer is governed by (e.g., Hopmans et al., 2002; Rau et al., 2012; Smith & Chapman, 1983)

$$D_x \frac{\partial^2 T}{\partial x^2} + D_y \frac{\partial^2 T}{\partial y^2} - q \frac{\rho_w c_w}{\rho c} \frac{\partial T}{\partial x} = \frac{\partial T}{\partial t} \tag{1}$$

where T [Θ] is the temperature in the aquifer, x and y [L] are the horizontal coordinates, t [T] is time, D_x and D_y [L^2T^{-1}] are the thermal dispersion coefficients in the x and y directions, respectively, q [LT^{-1}] is the specific discharge in the x direction, and ρc and $\rho_w c_w$ [$ML^{-1}T^{-2}\Theta^{-1}$] are the volumetric heat capacity of saturated soil and water, respectively. All parameters are constants that do not vary in space and time, such that the differential equation (equation (1)) is linear and solutions can be superimposed. The thermal dispersion coefficients consist of a thermal conduction term and a term that accounts for the effect of hydrodynamic dispersion in the water phase (e.g., De Marsily, 1986; Rau et al., 2012)

$$D_x = \frac{\kappa}{\rho c} + \beta_x q \frac{\rho_w c_w}{\rho c} \tag{2}$$

$$D_y = \frac{\kappa}{\rho c} + \beta_y q \frac{\rho_w c_w}{\rho c} \tag{3}$$

where κ [L^2MT^{-3}] is the isotropic bulk thermal conductivity and β_x and β_y [L] are the longitudinal and transverse thermal dispersivities, respectively, which are of the same order of magnitude as the solute transport dispersivities (De Marsily, 1986; Hopmans et al., 2002).

A vertical heating cable acts as a vertical line source located at the origin of the coordinate system. The cable produces a constant amount of heat per unit length p [MLT^{-3}] when turned on at time $t = 0$. The temperature is measured with respect to the background temperature and is initially zero everywhere and remains zero at infinity. The specific discharge is approximated as steady and uniform in each layer; the effect of the cables on the flow field is neglected. The differential equation (equation (1)) with the stated initial and boundary conditions and a point source at the origin of strength p was solved for solute transport by Hunt (1983), after which the analogy to heat transfer was made by Zubair and Chaudhry (1996) and Diao et al. (2004). The solution is written here as

$$T = \frac{p}{4\pi\rho c\sqrt{D_x D_y}} \exp\left(\frac{x}{B}\right) \mathrm{W}\left(\frac{A}{t}, \frac{r}{B}\right) \tag{4}$$

where

$$A = \frac{r^2}{4D_x} \tag{5}$$

$$B = 2D_x \frac{\rho c}{q \rho_w c_w} \tag{6}$$

$$r = \sqrt{x^2 + \frac{D_x}{D_y} y^2} \tag{7}$$

$$\mathrm{W}\left(\frac{A}{t}, \frac{r}{B}\right) = \int_{A/t}^{\infty} \frac{1}{s} \exp\left(-s - \frac{r^2}{4B^2 s}\right) \mathrm{d}s \tag{8}$$

where W is known in the groundwater literature as the Hantush Well function (Hantush, 1956). The corresponding steady state temperature, $T\left(t_\infty\right)$, is given by (Diao et al., 2004; Zubair & Chaudhry, 1996)

$$T\left(t_\infty\right) = \frac{p}{2\pi\rho c\sqrt{D_x D_y}} \exp\left(\frac{x}{B}\right) \mathrm{K}_0\left(\frac{r}{B}\right) \tag{9}$$

where K_0 is the modified Bessel function of the second kind and order 0. Combination of equations (4) and (9) gives

$$T(t) = \frac{T(t_\infty)}{2\mathrm{K}_0\left(\frac{r}{B}\right)} \mathrm{W}\left(\frac{A}{t}, \frac{r}{B}\right) \tag{10}$$

It is noted that half the steady state temperature is reached when $t = 2\frac{A}{r/B} = \frac{r\rho c}{q\rho_w c_w}$ (Wilson & Miller, 1978). The solution for a heat source that is turned on at $t = 0$ and turned off at $t = t_0$ is obtained from superposition as

$$T(t, t_0) = \begin{cases} \frac{T(t_\infty)}{2\mathrm{K}_0(r/B)} \mathrm{W}\left(\frac{A}{t}, \frac{r}{B}\right), & 0 < t \le t_0 \\ \frac{T(t_\infty)}{2\mathrm{K}_0(r/B)} \left[\mathrm{W}\left(\frac{A}{t}, \frac{r}{B}\right) - \mathrm{W}\left(\frac{A}{t-t_0}, \frac{r}{B}\right)\right], & t > t_0 \end{cases} \tag{11}$$

The temperature response presented in equation (11) is expressed as a function of three lumped parameters, A, $\frac{r}{B}$, and $T(t_\infty)$, which account for the position of the fiber-optic cable relative to the heating cable (x and y), and the parameters of the problem (q, ρc, $\rho_w c_w$, κ, β_x, β_y, and p).

The temperature response depends on the location of the measurement relative to the heat source. Example temperature responses at 1 cm downstream (blue crosses) and 1 cm upstream (orange diamonds) of the heat source are shown in Figure 1a. The two temperature responses are significantly different during the heating period but are similar after the heat source is turned off. The scaled temperature $\frac{T(t)}{T(t_\infty)}$ is plotted as a function of the scaled time $\frac{t}{A}$ in Figure 1b. The two temperature responses have the same A and $\frac{r}{B}$, such that they overlap in Figure 1b.

3. Estimation of Specific Discharge From Measurements

Values for the lumped parameters A, $\frac{r}{B}$, and $T(t_\infty)$ are obtained by fitting equation (11) to temperature measurements of a heat pulse response test as described in section 4. Note that these parameters can be obtained without knowledge of the exact position of the temperature measurement relative to the heat source. The specific discharge is obtained from A and $\frac{r}{B}$ by rewriting equation (6) as

$$q = 2D_x \frac{\rho c}{\rho_w c_w} \frac{1}{B} \tag{12}$$

Multiplication by $r/\sqrt{4D_x A}$, which equals one (equation (5)), gives

$$q = \frac{\rho c}{\rho_w c_w} \frac{r}{B} \frac{1}{\sqrt{A}} \sqrt{D_x} \tag{13}$$

Substitution of equation (2) for D_x finally gives

$$q = \frac{1}{\rho_w c_w} \frac{r/B}{\sqrt{A}} \sqrt{\rho c \left(\kappa + \beta_x q \rho_w c_w\right)} \tag{14}$$

The specific discharge q can now be determined from parameters A, $\frac{r}{B}$, and a third term. Note that A and $\frac{r}{B}$ are both functions of r, but the ratio $\frac{r/B}{\sqrt{A}} = \frac{q\rho_w c_w}{\rho c\sqrt{D_x}}$ does not depend on r, which makes the expression for the specific discharge independent of the position of the temperature measurement relative to the heat source. The term under the square root sign consists of a thermal conductivity component and a hydrodynamic dispersion component. Equation 14 may be solved explicitly for q by rewriting the equation

$$q = \frac{1}{\rho_w c_w}\left(\left[\frac{r/B}{\sqrt{A}}\right]^2 \frac{\beta_x \rho c}{2} + \frac{r/B}{\sqrt{A}}\sqrt{\kappa\rho c + \left[\frac{1}{2}\frac{r/B}{\sqrt{A}}\beta_x \rho c\right]^2}\right) \tag{15}$$

Equations (14) and (15) allow for the calculation of the specific discharge without knowledge of the position of the temperature measurement relative to the heat source by estimating $\frac{r/B}{\sqrt{A}}$, $\rho_w c_w$, $\kappa\rho c$, and $\beta_x \rho c$. Approximate values and distributions for the thermal properties of saturated sand with a porosity of 0.35 are used for Case Studies I and II (Table 1). The thermal dispersivity β_x has the largest uncertainty. Similar to solute dispersivity, the thermal dispersivity is scale dependent (De Marsily, 1986). Reported values range from 0.002 m for a heat pulse probe experiment (Hopmans et al., 2002), to 0.1 m for a push-pull pumping test (Vandenbohede et al., 2009), to 1 m for a closed geothermal system (Molina-Giraldo et al., 2011). The scale of the presented heat pulse test is somewhere between the heat probe experiment of Hopmans et al. (2002) and the push-pull pumping test of Vandenbohede et al. (2009). The distribution of β_x used to estimate the distribution of $\beta_x \rho c$ in Table 1 is lognormal with a 95% confidence interval between 0.01 and 0.16 m.

4. Curve Fitting Procedure

The temperature response is measured with DTS along the fiber-optic cable and is normalized by subtracting the background temperature. Temperature measurements are representative for short sections of the cable. The pulse response for each section is described by equation (11). The parameters $T(t_\infty)$, A, and $\frac{r}{B}$ for each of these sections are estimated from the measured temperature response with the curve fitting procedure described below. The residuals, ε [Θ], are the differences between modeled and measured temperatures. The root-mean-square error, RMSE [Θ], is defined as

$$\mathrm{RMSE} = \sqrt{\frac{\sum_{t=1}^{m} \varepsilon_t^2}{m}} \tag{16}$$

where m is the number of time steps.

The residuals are likely correlated in time. A first-order autoregressive model is used to remove the autocorrelation in the residuals

$$\varepsilon_t = \alpha \varepsilon_{t-1} + n_t \tag{17}$$

where α [-] is the autoregressive parameter and n_t [Θ] is the remaining noise at time step t. The noise is approximated as independent and identically distributed. The parameters $T(t_\infty)$, A, $\frac{r}{B}$, and α are estimated by minimizing the RMS noise

$$\mathrm{RMSN} = \sqrt{\frac{\sum_{t=2}^{m} n_t^2}{m-1}} = \sqrt{\frac{\sum_{t=2}^{m} \left(\varepsilon_t - \alpha\varepsilon_{t-1}\right)^2}{m-1}} \tag{18}$$

Table 1
Values for the Thermal Properties Used for Case Studies I and II

Parameter	Estimated distribution	Units
$\rho_w c_w$	4.185	$MJm^{-1}°C^{-1}$
$\kappa\rho c$	$N(\mu = 566, \sigma = 15.7)$	$GJ^2d^{-1}m^{-2}°C^{-2}$
$\beta_x\rho c$	$LogN(\mu = 0.137, \sigma = 0.110)$[a]	$MJ°C^{-1}$

[a]Ninety-five percent of the lognormal distribution lies between 0.027 and 0.425 MJ/°C

The RMSN is minimized with a Levenberg-Marquardt algorithm (Marquardt, 1963) using `LMFIT` (Newville et al., 2014), a high-level Python interface to the `scipy.optimize` module (Jones et al., 2001). A Monte Carlo analysis is performed in three steps to estimate the uncertainty of the estimated specific discharge. First, the covariance matrix is estimated for the parameters A, $\frac{r}{B}$, $T(t_\infty)$, and α. Second, a set of 10^6 parameter combinations is drawn from a multivariate normal distribution. Parameter sets of $\kappa\rho c$ and $\beta_x\rho c$ are drawn independently from the distributions presented in Table 1. Third, the specific discharge is calculated for each of the parameter combinations with equation (15), and the 2.5th and 97.5th percentiles are used for the 95% confidence interval. The estimation of the confidence interval assumes the thermal response is correctly approximated by equation (15). A Jupyter notebook with the curve fitting procedure and test data is provided as supporting information.

5. Case Studies

The presented approach is applied to two case studies. It is tested in Case Study I, which uses the data from Bakker et al. (2015). The range of applicability is explored in Case Study II, where the cables are installed much deeper, the specific discharge is a lot smaller and varies more with depth.

5.1. Case Study I: Dunes Near Castricum

The objective of Case Study I is to test the presented approach when the temperature response is measured at different positions relative to the heating cable. Use is made of the data set described in Bakker et al. (2015), who conducted an active heat pulse response test at a managed aquifer recharge system in the coastal dune area near Castricum, the Netherlands. Water flows from elongated infiltration basins over a distance of 80 m to a row of shallow wells parallel to these basins; the median residence time is approximately 50 days (Des Tombe et al., 2018). Fiber-optic cables were inserted with direct-push equipment at six locations; at location 2 the fiber-optic cable is accompanied by a heating cable (Figure 2). The fiber-optic cable is 6 mm thick, contains two multimode 50/125-μm fibers, and is heavily reinforced to protect the fibers during installation. The heating cable is an off-the-shelf model that is 7 mm thick and produces 30 W/m. The cables at location 2 reached a depth of 21 m below surface level, while the others reached a depth of 15 m. The heating cable was surrounded by multiple closely spaced fiber-optic cables to determine both the magnitude and direction of the velocity, but the direction is not considered in this paper. The position of each cable relative to the heating cable is known at the surface (Figure 2) but unknown at depth, as the cables were inserted with direct push, which gives small deviations from the vertical that were not measured.

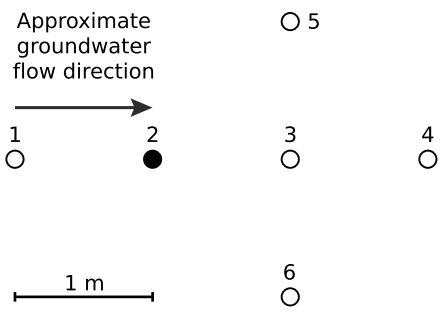

Figure 2. Top view of Case Study I. The circles represent the locations of the fiber-optic cables at the surface. The heating cable is located at the filled circle.

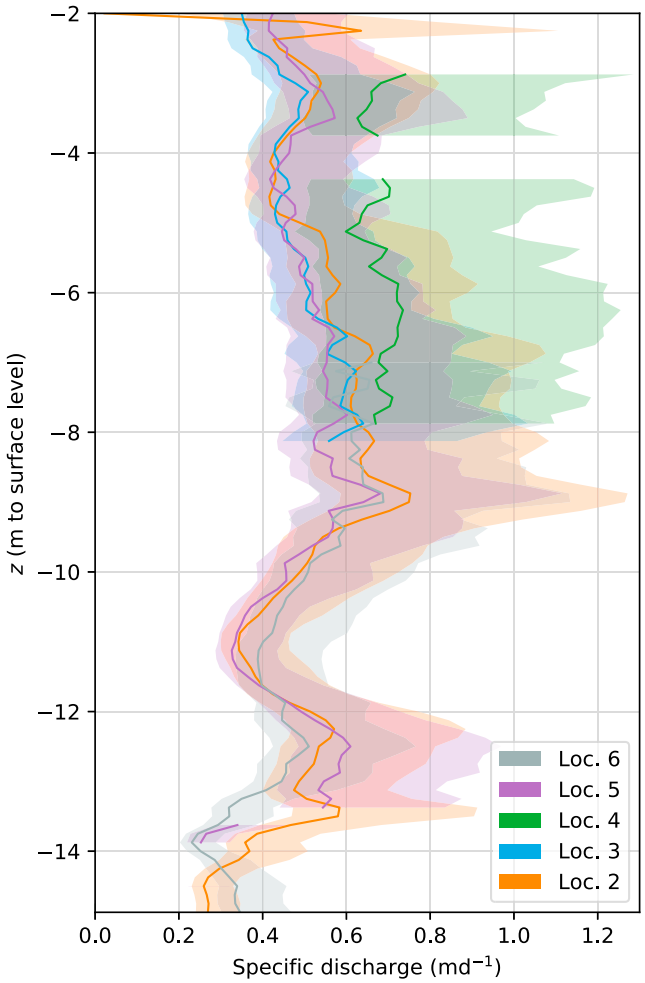

Figure 3. The specific discharge (line) and the 95% confidence intervals (shaded) estimated for locations 2–6 of Case Study I, at depths where the measured temperature increase was at least 0.5 °C.

A heat pulse of 30 W/m was generated for 3.8 days and the response was measured with DTS for 8.4 days with an acquisition time of 10 min on a 25-cm sampling interval. The Silixa Ultima was used with a spatial resolution of 0.29 m and a factory-reported accuracy of 0.02 °C corresponding to the 10 minute acquisition time and the total fiber length. The measurements in the first 10 min after the heating cable is turned on ($t = 0$) and off ($t = 3.8$ d) are excluded from the fitting procedure. The model is unable to simulate these measured temperatures, because both the heating cable and the fiber-optic cable are approximated as infinitely thin in the model. However, their thickness is finite and their volumetric heat capacity is different than that of the surrounding soil, which influences the short-term temperature response measured in the fiber-optic cable.

A good fit was obtained for each cable at all depths with a RMSE of 0.03–0.09 °C. The vertical variation in specific discharge and the 95% confidence intervals are estimated from the temperature measurements with respect to the background temperature at six locations with the procedure described in section 4 and are shown in Figure 3. The mean width of the 95% confidence interval is 0.33 m/day for all locations except location 4, where it is 0.60 m/day. As the system is shallow, with a short residence time, the background temperature varied slightly during the experiment. A linear interpolation between the first and last temperature measurement was performed to account for the variation in background temperature. The error introduced by the approximation of the background temperature resulted in unrealistic values for the estimated specific discharge with a large confidence interval at depths where the temperature increase remained below 0.5 °C during the test; these are not shown in Figure 3. The temperature response at location 1 (upstream of the heating cable) remained below this threshold and is therefore not shown in Figure 3.

A similar specific discharge is estimated for each of the cables and the 95% confidence intervals are close to each other or overlap, even though the positions of the fiber-optic cables relative to the heating cable were unknown and vary between being next to the heating cable (location 2, orange line in Figure 3) up to several meters from the heating cable (locations 3–6). A slightly higher specific discharge, together with a larger confidence interval, is calculated for location 4 (green line). A qualitative estimate for the specific discharge is obtained from Des Tombe et al. (2018) by dividing the distance between the recharge basin and the extraction well (80 m) by the median of the residence time (50 days) and multiplying it by the porosity (0.35), resulting in an estimate of 0.56 m/day. Bakker et al. (2015) estimated a pore water velocity profile (Figure 6 in their paper), which is similar to the specific discharge profile (Figure 3 of this paper) when multiplied with the porosity. It is noted that Bakker et al. (2015) did not account for thermal dispersion, which affects the estimate of the specific discharge significantly for this case (see section 6.2).

5.2. Case Study II: Horstermeer Polder

The objective of Case Study II is to explore the range of applicability of the proposed approach. It is investigated whether the specific discharge can be measured over larger depth (up to 45 m) and whether vertical variations of the specific discharge can be measured accurately. This case study is located in the Horstermeer polder in the Netherlands, which is an approximately circular polder with a diameter of 3 km. The heating cable and fiber-optic cable are installed at the edge of the polder, 50 m from the surrounding lakes and canals. The water level in the polder is maintained at approximately 2 m below the surrounding lakes and canals, resulting in significant groundwater flow from the lakes and canals into the polder. The cover layer is approximately 1.5 m thick and is very heterogeneous, while the aquifer below consists of different types of sands. Van Wielink (2016) showed with geophysical methods and through numerical modeling that horizontal flow is significantly larger at a depth between 25 and 35 m.

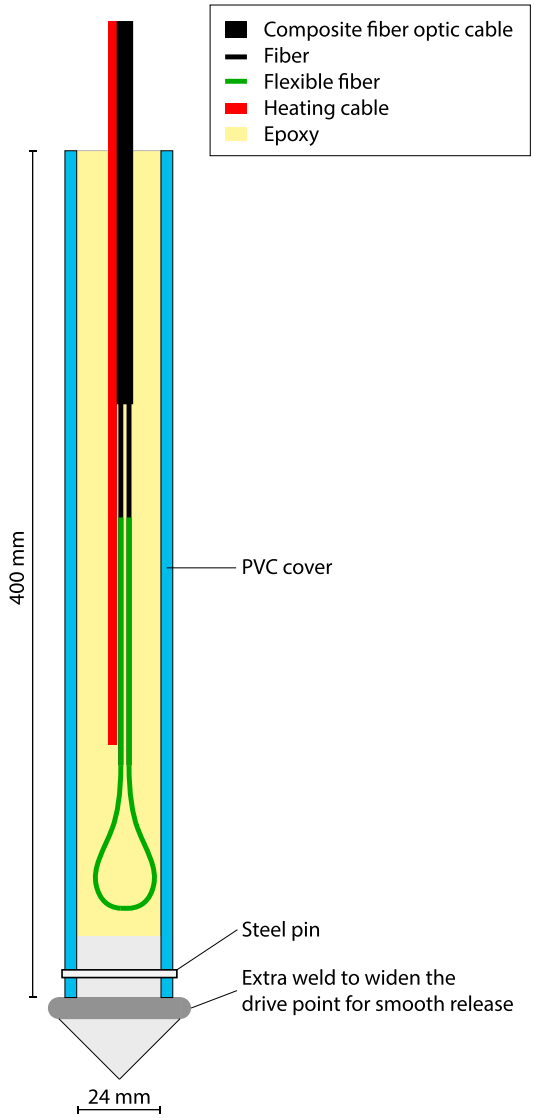

Figure 4. Custom made drive point. Not to scale. PVC = polyvinyl chloride.

Installation of the fiber-optic cables was modified from the approach used in Case Study I (Bakker et al., 2015). Thinner push rods were used to reach a depth of 45 m, but these only fit a single composite fiber-optic cable and a heating cable. The same fiber-optic cable was used as in Case Study I, which contains two fibers. Their endings are welded together with a flexible fiber near the drive point (Figure 4) to support double-ended DTS calibration (Van de Giesen et al., 2012). A plastic cover is attached to the steel drive point and filled with epoxy to fix the fragile fibers and the heating cable. A thinner heating cable with a diameter of 5 mm was installed (compared to Case Study I), which can generate a heat pulse of 20 W/m. In contrast to Case Study I, the heating and fiber-optic cables were not taped together but were kept loose during installation. Slack tends to occur in one of the cables when they are taped together, making it more difficult to lace the cables through the push rods. Alternatively, a fiber-optic cable with an embedded resistance wire could have been used. This has the advantage of being easier to install but may cause problems with getting too hot and was not investigated.

The heat pulse was generated for 4.8 days. The temperature response along the fiber-optic cable was measured with the Silixa Ultima for 10.9 days with an acquisition time of 5 min on a 0.125-m sampling interval. The factory-reported temperature accuracy is 0.024 °C. The pulse response over the depth is shown in Figure 5a. The temperature measurements in the first 2 m below surface level reflect partially saturated soils and are influenced by surface temperature fluctuations; their interpretation is beyond the scope of this paper.

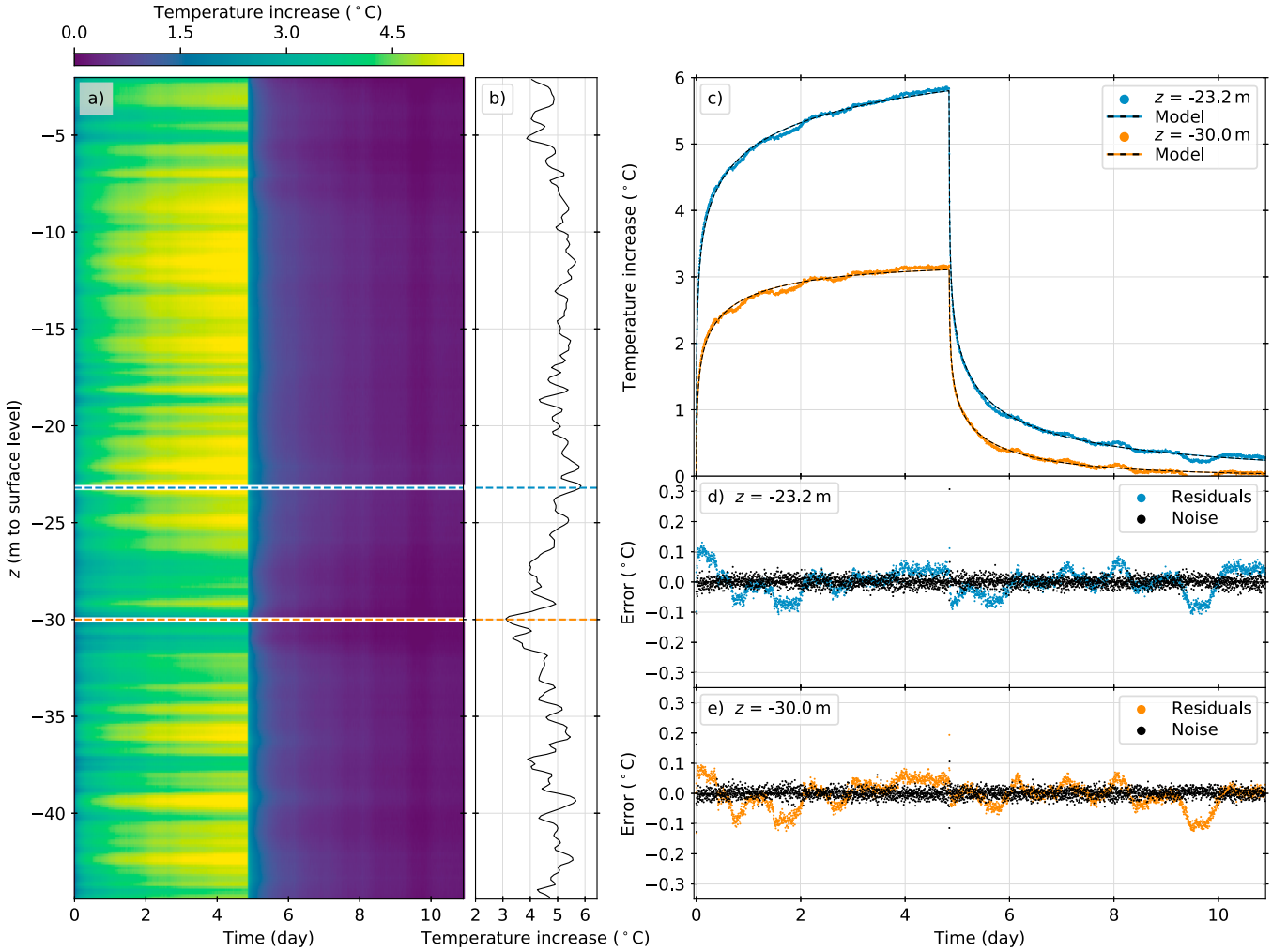

Figure 5. (a) Measured temperature response for Case Study II. (b) Temperature profile at $t = 4.8$ days, just before the heating cable was turned off. (c) Measured and modeled temperature response at two depths. (d, e) Residuals and noise at two depths.

The thermal properties of the drive point are different than that of the aquifer, which influences the temperature measurements in the bottom 2 m and are therefore not shown in Figure 5a. The temperature increase just before the heating cable was turned off is shown in Figure 5b. The largest temperature increase of 5.9 °C is observed at 23.2 m below surface level and the smallest increase of 3.1 °C at 30 m below surface level. The temperature increase fluctuates with depth, as the fiber-optic cable twists around the heating cable and the temperature increase just upstream of the heating cable is significantly smaller than just downstream (Figure 1a).

The specific discharge was estimated with the procedure presented in section 4. A good fit was obtained at all depths with a RMSE of 0.04–0.05 °C. The measured (dots) and modeled (dashed lines) temperature responses at 23.2 (blue) and 30 m (orange) below surface level are shown in Figure 5c; the corresponding residuals are shown with colored dots in Figures 5d and 5e, respectively. The temporal variation in the residuals is similar at all depths and shows a daily pattern originating from the DTS system. The noise (equation (17)), shown with black dots in Figures 5d and 5e, does not show this temporal variation and is distributed approximately normal. Similar to Case Study I, the measurements in the first 10 min after the heating cable is turned on ($t = 0$) and off ($t = 4.8$ days) are excluded from the fitting procedure. The estimated specific discharge and its 95% confidence interval are shown in Figure 6. The mean width of the 95% confidence interval is 0.026 m/day. The specific discharge varies between 0.07 and 0.11 m/day, except for the first 8 m and between 27 and 32 m below surface level, where the specific discharge is larger, as was

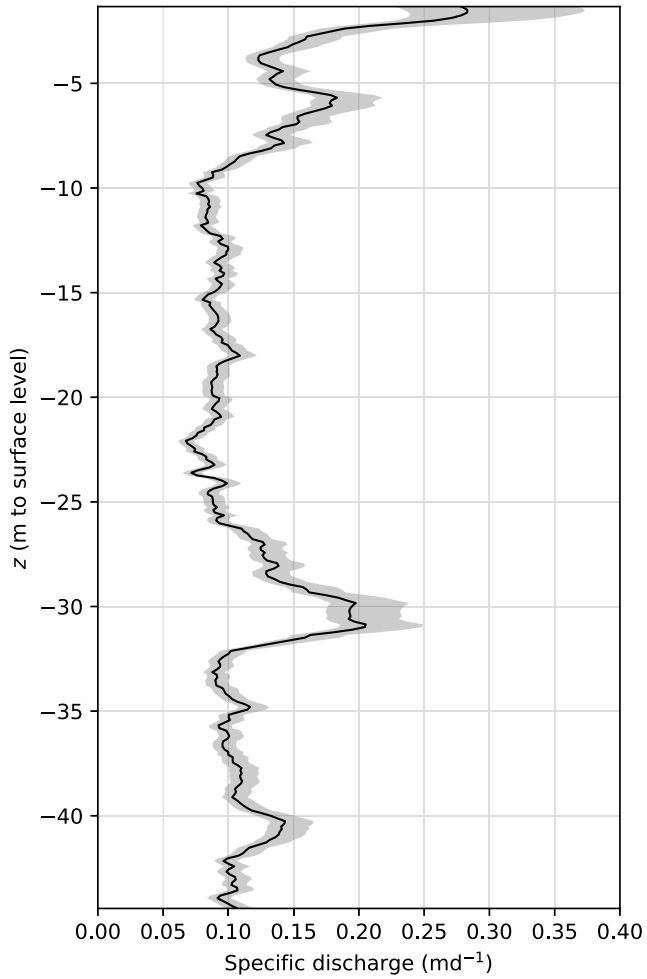

Figure 6. The specific discharge and its 95% confidence interval estimated for Case Study II.

expected from the geophysical study and numerical modeling of Van Wielink (2016). The largest specific discharge of 0.2 m/day is estimated at 31 m below surface level.

6. Discussion

Several approximations were made to estimate the specific discharge from the temperature measurements of which three require extra attention and are discussed below.

6.1. Vertical Conductive Heat Transfer

In the presented approach the aquifer is discretized vertically in many horizontal layers. The temperature measurements in each layer are considered independent from the other layers and heat transfer between layers is neglected. If there is a large difference in the specific discharge between two layers, a temperature difference develops during the test and heat is exchanged vertically by means of conduction. This is neglected in the presented approach. If vertical heat transfer is not negligible, sharp changes in the specific discharge and thin layers with a different specific discharge can be missed. A sharp change in the specific discharge is estimated for Case Study II at approximately 28–32 m below surface level, and the question arises whether the maximum specific discharge at this depth is correctly estimated.

A numerical model was constructed to investigate the effect of vertical heat conduction on the estimated specific discharge. An aquifer is modeled with a constant horizontal specific discharge of 0.1 m/day, except for a layer where the specific discharge is higher (q_f). The layer is located halfway the aquifer and has a thickness H. A 20 W/m vertical line source is located at the origin and is turned on at the beginning of the model run and turned off after 4.8 days. Other parameters are given in Table 2. Coupled groundwater flow

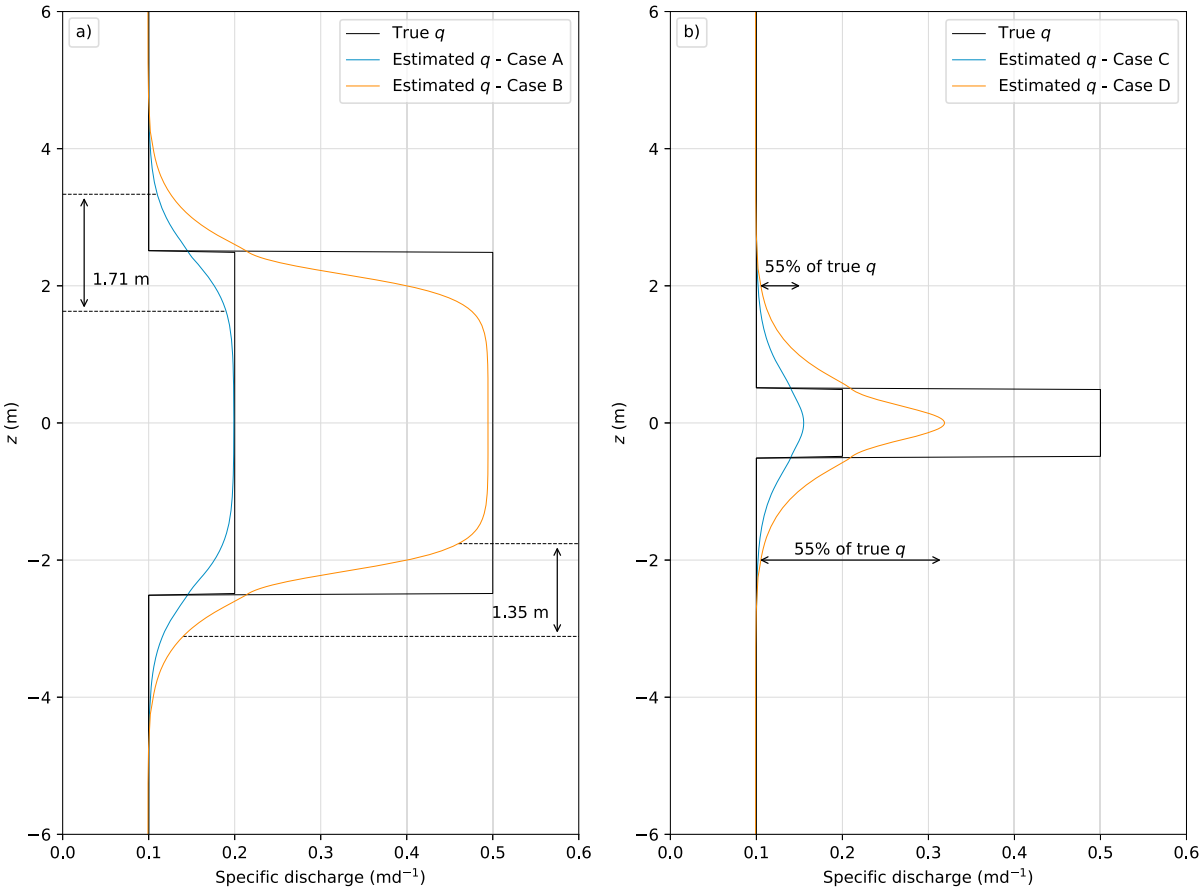

Figure 7. (a) True (black) and estimated specific discharge for Case A (blue) and Case B (orange). (b) True (black) and estimated specific discharge for Case C (blue) and Case D (orange).

and heat transfer are modeled with SEAWAT (Langevin et al., 2007). The equations for thermal conduction and hydrodynamic dispersion are solved with an implicit finite difference scheme and the thermal advection is solved using a third-order total-variation-diminishing scheme (Zheng & Wang, 1999). The cell sizes vary from 0.5 × 0.5 × 2.5 cm to 1 × 1 × 1 m (x, y, and z). The smallest cells are used at the origin near the top and bottom of the layer with larger specific discharge, while the largest cells are used near the boundaries of the model.

The temperature response is modeled for two values of q_f and two values of H, resulting in four cases labeled A–D (Table 3). The specific discharge is estimated from the modeled temperature at 2 cm from the heating cable perpendicular to the flow direction using the presented approach. Results are shown with blue and orange lines in Figure 7, which also shows the true specific discharge (black). A similar specific discharge

Table 2
Parameters Used in the Numerical Model

Parameter	Value
ρc	2.730 MJm^{-1}°C^{-1}
$\rho_w c_w$	4.185 MJm^{-1}°C^{-1}
κ	2.4 Wm^{-1}°C^{-1}
β_x	0.05 m
β_y	0.005 m
β_z	0.0005 m

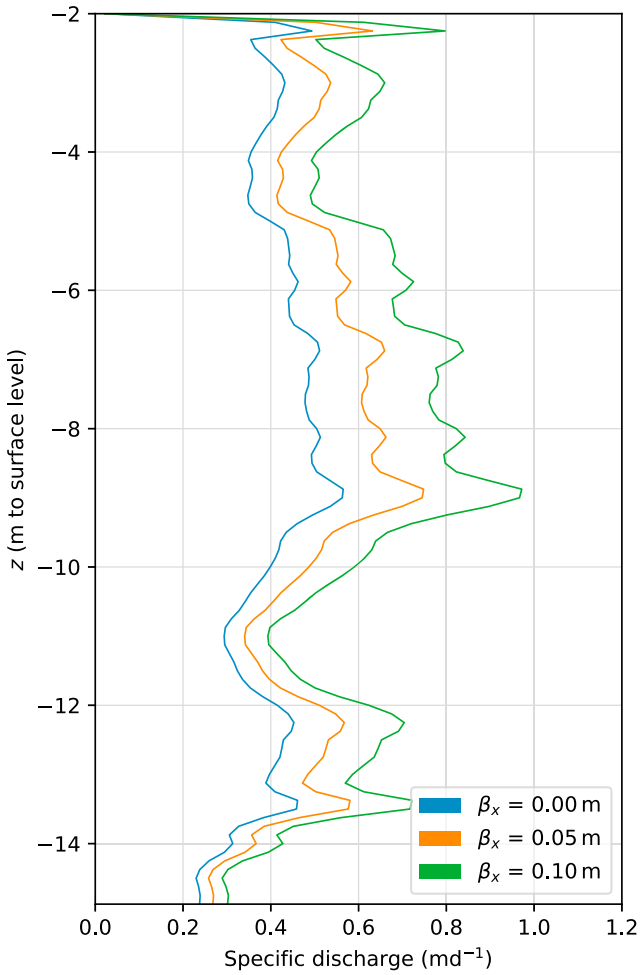

Figure 8. The specific discharge for three values of β_x for location 2 of Case Study I.

is estimated from modeled temperatures at 2 cm upstream and 2 cm downstream of the heating cable (not shown).

The true specific discharge jumps at the boundary of the layer with higher q_f, while the estimated specific discharge shows a smooth transition. The height of the transition zone, from 10% to 90% of the total increase, is termed the spatial resolution of the estimated specific discharge here. The spatial resolution for $q_f = 0.2$ m/day (Case A) is 1.71 m and reduces to 1.35 m for $q_f = 0.5$ m/day (Case B). For Cases A and B, the layer thickness is 5 m, which is larger than the spatial resolution, so that the largest estimated specific discharge approximates the true specific discharge quite well. When the layer thickness is smaller than the spatial resolution (Cases C and D), the peak of the specific discharge is underestimated. For example, when $H = 1$ m (Cases C and D) the peak of the estimated specific discharge is only 55% of the true specific discharge (Figure 7b).

Table 3
Numerical Model Configurations

Case	q_f (m/day)	H (m)
A	0.2	5.0
B	0.5	5.0
C	0.2	2.0
D	0.5	2.0

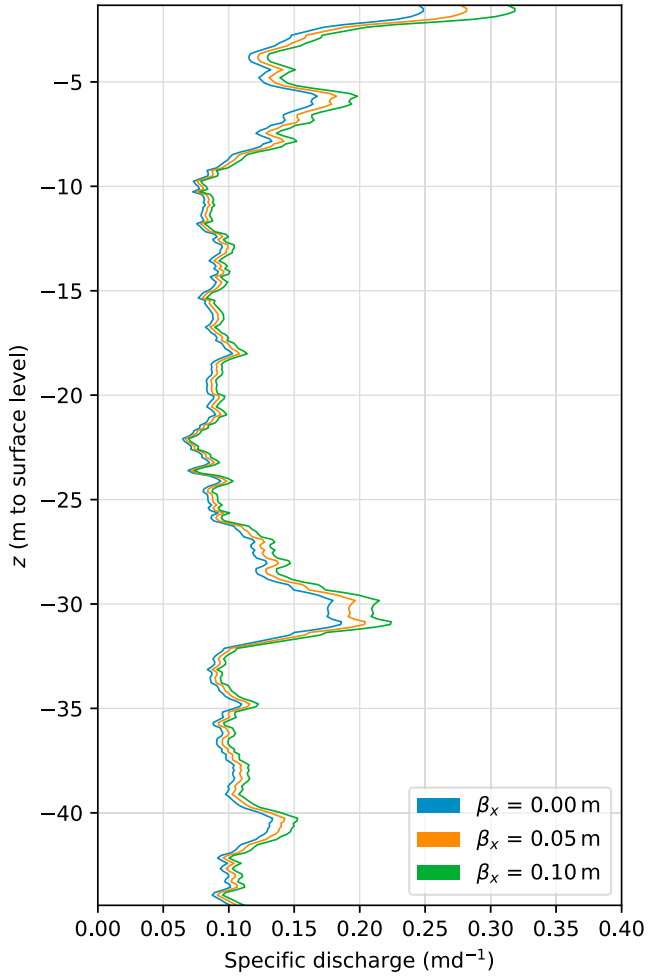

Figure 9. The specific discharge for three values of β_x for Case Study II.

The thickness of the region with a larger specific discharge of Case Study II is approximately 4 m (between 28 and 32 below surface level) and thus larger than the spatial resolution of the estimated specific discharge. It is therefore expected that the peak specific discharge in this layer is estimated reasonably well, but the estimated transition of the specific discharge is likely smoother than in reality.

6.2. Hydrodynamic Dispersion

The parameters A, r/B, and T_∞ are obtained from temperature measurements with the curve fitting procedure presented in section 4. In addition, estimates of $\kappa\rho c$, $\beta_x\rho c$, and $\rho_w c_w$ (equation (15)) are needed to calculate the specific discharge. The estimate of the specific discharge increases for larger β_x, and the increase is larger for a larger specific discharge. Similar observations were made in studies by Hopmans et al. (2002) and Lu et al. (2018). The effect of hydrodynamic dispersion can be neglected when $\kappa \gg \beta_x q \rho_w c_w$ (equation (14)) or

$$q \ll \frac{\kappa}{\beta_x \rho_w c_w} \tag{19}$$

The condition for neglecting hydrodynamic dispersion with the values of Table 2 becomes

$$q\beta_x \ll 0.05\,\mathrm{m}^2/\mathrm{day} \tag{20}$$

The uncertainty in β_x is much larger than the uncertainty in κ and $\rho_w c_w$. This makes it difficult to decide for what values of q dispersion can be neglected. For $\beta_x = 0.05$ m (Table 2), dispersion may be neglected when $q \ll 1$ m/day.

The term under the square root sign in equation (14) reduces to $\sqrt{\kappa\rho c}$ when hydrodynamic dispersion is neglected, so that equation (14) can be written as

$$q = \frac{\sqrt{\kappa\rho c}}{\rho_w c_w}\frac{r/B}{\sqrt{A}} \tag{21}$$

$$\approx 0.18\,\frac{r/B}{\sqrt{A}}\,(\mathrm{m/day}) \tag{22}$$

The term $\sqrt{\kappa\rho c}$ is relatively constant for different types of saturated sand, because either a larger porosity or a larger clay content results in a larger ρc and a lower κ.

The specific discharge is estimated for location 2 of Case Study I (next to the heating cable) for three values of β_x, and the results are shown in Figure 8. The estimated specific discharge is significantly larger when $\beta_x = 0.1$ m (green) than when hydrodynamic dispersion is neglected ($\beta_x = 0$ m, blue), as is to be expected as q is around 0.5 m/day. For example, the estimated specific discharge is 72% larger at 9 m below surface level for $\beta_x = 0.1$ m than for $\beta_x = 0$ m. The effect of hydrodynamic dispersion on the estimated specific discharge is much smaller for Case Study II (Figure 9), with a maximum increase of 20% at 31 m below surface level. This is to be expected as $q = 0.1$–0.2 m/day $\ll 1$ m/day. The same holds for the confidence intervals of the estimated specific discharge presented in Figures 3 and 6; the confidence intervals are wider for large flows due to the uncertainty in the dispersivity.

6.3. Heterogeneity in Horizontal Layers

In this study, effective values of $\rho_w c_w$, $\kappa\rho c$, and $\beta_x \rho c$ for the measurement area are used to estimate an effective value of q. The size of the measurement area is estimated by calculating the area that is heated at least 0.1 °C during the test. The measurement area is approximately 5.9 m^2 if the specific discharge is 0.1 m/day and 8.3 m^2 if the specific discharge is 0.5 m/day, using the values of Table 2 and a heat pulse of 4.8 days. Not all parts of the measurement area contribute equally to the estimate of the effective q. Knight et al. (2007) assessed the effect of heterogeneity on the estimation of the heat capacity and water content in the vadose zone with a dual-probe heat pulse sensor. They concluded that the measurements are local and the area close to the heater and the sensor contributes most. Oliver (1993) performed a similar assessment for a pumping test by quantifying the influence of the storativity and transmissivity at each location on the observed drawdown. He concluded that at later times the influence extends farther away from the well and the effective values represent a larger area. Future research into the combined effect of heterogeneity and test duration is needed to understand the full effect of heterogeneity on the estimated effective values.

7. Conclusion

A new approach is presented to estimate the specific discharge from a heat pulse response test using a heating cable and a single fiber-optic cable. The temperature is measured along the fiber-optic cable with a DTS system. The two cables are installed together with direct-push equipment, such that the cables are in direct contact with the aquifer and no borehole is needed; it is assumed that the disturbance of the flow field due to installation is neglected. Bakker et al. (2015) found that the cables twist when they are installed together, such that the position of the fiber-optic cable relative to the heating cable in the subsurface is unknown. The presented approach can be used to estimate the magnitude of the specific discharge independent of the position of the fiber-optic cable relative to the heating cable.

The aquifer is discretized vertically in many horizontal layers. Each layer is approximated as homogeneous with a uniform flow perpendicular to the heating cable. The temperature response in each layer is fitted with three lumped parameters, from which the specific discharge is calculated by estimating a conduction term and a hydrodynamic dispersion term. The conduction term appears to be relatively constant for different types of sand. Hydrodynamic dispersion can be neglected when the specific discharge is significantly smaller than 1 m/day. The estimate of the specific discharge increases for a larger longitudinal thermal dispersivity. The uncertainty in the dispersivity results in larger uncertainty in the estimation of larger specific discharge values.

The new approach was successfully tested in Case Study I using data of Bakker et al. (2015). In Case Study II it was demonstrated that smaller values of the specific discharge (~0.1 m/day) can be measured accurately over larger depth (~45 m) including a region with significantly higher specific discharge (~0.2 m/day).

Vertical heat transfer between layers is neglected in the presented approach to estimate the specific discharge from the measured temperature response. The estimated specific discharge is smoother than in reality near jumps in the specific discharge. It was concluded from a 3-D numerical model that the sharp increase in the specific discharge in Case Study II results in a smooth transition in the estimate of the specific discharge over a distance of 1.35–1.71 m, termed the spatial resolution of the presented approach. The specific discharge in layers that are thinner than the spatial resolution are not fully captured. The layer in Case Study II where the specific discharge is larger is thick enough (~4 m) that the peak flow in this layer is captured. Results at a finer resolution than the spatial resolution require the use of a 3-D model that accounts for vertical heat transfer to estimate the specific discharge from the measured temperature response.

Acknowledgments
All temperature measurements and derived estimates are available at https://doi.org/10.5281/zenodo.1436300. This work was funded in part by the Netherlands Organization for Scientific Research (NWO) within the program the New Delta with project number 869.15.006, and by Waternet, the Water Authority Amstel, Gooi and Vecht, the Municipality of Amsterdam, and the Province of Noord-Holland. The authors thank Tom Kind from Waternet for his assistance with the experimental setup of Case Study II. This manuscript was improved by the constructive suggestion of three anonymous reviewers.

References

Anderson, M. P. (2005). Heat as a ground water tracer. *Groundwater*, *43*(6), 951–968. https://doi.org/10.1111/j.1745-6584.2005.00052.x

Bakker, M., Caljé, R., Schaars, F., Van der Made, K., & de Haas, S. (2015). An active heat tracer experiment to determine groundwater velocities using fiber optic cables installed with direct push equipment. *Water Resources Research*, *51*, 2760–2772. https://doi.org/10.1002/2014WR016632

Banks, E. W., Shanafield, M. A., Noorduijn, S., McCallum, J., Lewandowski, J., & Batelaan, O. (2018). Active heat pulse sensing of 3-D-flow fields in streambeds. *Hydrology and Earth System Sciences*, *22*(3), 1917–1929. https://doi.org/10.5194/hess-22-1917-2018

Bense, V. F., Read, T., Bour, O., Le Borgne, T., Coleman, T., Krause, S., et al. (2016). Distributed temperature sensing as a downhole tool in hydrogeology. *Water Resources Research*, *52*, 9259–9273. https://doi.org/10.1002/2016WR018869

Bredehoeft, J. D., & Papadopulos, I. S. (1965). Rates of vertical groundwater movement estimated from the Earth's thermal profile. *Water Resources Research*, *1*(2), 325–328. https://doi.org/10.1029/WR001i002p00325

Cartwright, K. (1970). Groundwater discharge in the Illinois basin as suggested by temperature anomalies. *Water Resources Research*, *6*(3), 912–918. https://doi.org/10.1029/WR006i003p00912

Chiasson, A., Rees, S., & Spitler, J. (2000). A preliminary assessment of the effects of groundwater flow on closed-loop ground source heat pump systems. *ASHRAE Transactions*, *106*(1), 380–393.

Coleman, T. I., Parker, B. L., Maldaner, C. H., & Mondanos, M. J. (2015). Groundwater flow characterization in a fractured bedrock aquifer using active DTS tests in sealed boreholes. *Journal of Hydrology*, *528*, 449–462. https://doi.org/10.1016/j.jhydrol.2015.06.061

De Marsily, G. (1986). *Quantitative hydrogeology: Groundwater hydrology for engineers.* Cambridge, MA: Academic Press.

Des Tombe, B. F., Bakker, M., Schaars, F., & Van der Made, K.-J. (2018). Estimating travel time in bank filtration systems from a numerical model based on DTS measurements. *Groundwater*, *56*(2), 288–299. https://doi.org/10.1111/gwat.12581

Diao, N., Li, Q., & Fang, Z. (2004). Heat transfer in ground heat exchangers with groundwater advection. *International Journal of Thermal Sciences*, *43*(12), 1203–1211. https://doi.org/10.1016/j.ijthermalsci.2004.04.009

Domenico, P., & Palciauskas, V. (1973). Theoretical analysis of forced convective heat transfer in regional ground-water flow. *Geological Society of America Bulletin*, *84*(12), 3803–3814.

Drost, W., Klotz, D., Koch, A., Moser, H., Neumaier, F., & Rauert, W. (1968). Point dilution methods of investigating ground water flow by means of radioisotopes. *Water Resources Research*, *4*(1), 125–146. https://doi.org/10.1029/WR004i001p00125

Drury, M., Jessop, A., & Lewis, T. (1984). The detection of groundwater flow by precise temperature measurements in boreholes. *Geothermics*, *13*(3), 163–174. https://doi.org/10.1016/0375-6505(84)90013-0

Greswell, R. B., Riley, M. S., Alves, P. F., & Tellam, J. H. (2009). A heat perturbation flow meter for application in soft sediments. *Journal of Hydrology*, *370*(1-4), 73–82. https://doi.org/10.1016/J.JHYDROL.2009.02.054

Hantush, M. S. (1956). Analysis of data from pumping tests in leaky aquifers. *Eos, Transactions American Geophysical Union*, *37*(6), 702–714. https://doi.org/10.1029/TR037i006p00702

Hopmans, J. W., Šimunek, J., & Bristow, K. L. (2002). Indirect estimation of soil thermal properties and water flux using heat pulse probe measurements: Geometry and dispersion effects. *Water Resources Research*, *38*(1), 1006. https://doi.org/10.1029/2000WR000071

Hunt, B. (1983). *Mathematical analysis of groundwater resources* (pp. 124–152). London, Boston: Butterworth-Heinemann. https://doi.org/10.1016/B978-0-408-01399-4.50009-3

Jones, E., Oliphant, T., & Peterson, P. (2001). SciPy: Open source scientific tools for Python. Retrieved from http://www.scipy.org/; accessed November, 2017; Version 1.0.0.

Kluitenberg, G. J., Bristow, K. L., & Das, B. S. (1995). Error analysis of heat pulse method for measuring soil heat capacity, diffusivity, and conductivity. *Soil Science Society of America*, *59*(January), 719–726. https://doi.org/10.2136/sssaj1995.03615995005900030013x

Knight, J. H., Jin, W., & Kluitenberg, G. J. (2007). Sensitivity of the dual-probe heat-pulse method to spatial variations in heat capacity and water content. *Vadose Zone Journal*, *6*(4), 746–758. https://doi.org/10.2136/vzj2006.0170

Langevin, C. D., Thorne, D. T. Jr., Dausman, A. M., Sukop, M. C., & Guo, W. (2007). SEAWAT version 4: A computer program for simulation of multi-species solute and heat transport, *U.S. Geological Survey Techniques and Methods Book 6* (Chap. A22, pp. 39). Reston: U.S. Geological Survey.

Leaf, A. T., Hart, D. J., & Bahr, J. M. (2012). Active thermal tracer tests for improved hydrostratigraphic characterization. *Ground Water*, *50*(5), 726–735. https://doi.org/10.1111/j.1745-6584.2012.00913.x

Lu, X.-r., Sun, Y., Chen, G.-s., Qin, Y., Bai, Y.-f., Li, X.-j., & Mou, X.-j. (2018). Influences of thermal dispersion on soil water flux estimates using heat pulse technique in saturated soils. *CATENA*, *167*, 228–235. https://doi.org/10.1016/J.CATENA.2018.04.041

Marquardt, D. W. (1963). An algorithm for least-squares estimation of nonlinear parameters. *Journal of the Society for Industrial and Applied Mathematics*, *11*(2), 431–441. https://doi.org/10.1137/0111030

Molina-Giraldo, N., Bayer, P., & Blum, P. (2011). Evaluating the influence of thermal dispersion on temperature plumes from geothermal systems using analytical solutions. *International Journal of Thermal Sciences*, *50*(7), 1223–1231. https://doi.org/10.1016/j.ijthermalsci.2011.02.004

Moscoso Lembcke, L. G., Roubinet, D., Gidel, F., Irving, J., Pehme, P., & Parker, B. L. (2015). Analytical analysis of borehole experiments for the estimation of subsurface thermal properties. *Advances in Water Resources*, *91*, 88–103. https://doi.org/10.1016/j.advwatres.2016.02.011

Newville, M., Stensitzki, T., Allen, D. B., & Ingargiola, A. (2014). LMFIT: Non-linear least-square minimization and curve-fitting for Python. https://doi.org/10.5281/zenodo.11813

Oliver, D. S. (1993). The influence of nonuniform transmissivity and storativity on drawdown. *Water Resources Research*, *29*(1), 169–178. https://doi.org/10.1029/92WR02061

Pehme, P., Parker, B., Cherry, J. A., & Greenhouse, J. P. (2007). The potential for compromised interpretations when based on open borehole geophysical data in fractured rock. In *Proc. EPA/NGWA Fractured Rock Conference: State of the Science and Measuring Success in Remediation* (pp. 24–26). Portland, Maine.

Pehme, P., Parker, B., Cherry, J., & Greenhouse, J. (2010). Improved resolution of ambient flow through fractured rock with temperature logs. *Ground Water*, *48*(2), 191–205. https://doi.org/10.1111/j.1745-6584.2009.00639.x

Rau, G. C., Andersen, M. S., & Acworth, R. I. (2012). Experimental investigation of the thermal dispersivity term and its significance in the heat transport equation for flow in sediments. *Water Resources Research*, *48*, W03511. https://doi.org/10.1029/2011WR011038

Read, T., Bour, O., Selker, J. S., Bense, V. F., Borgne, T. L., Hochreutener, R., & Lavenant, N. (2014). Active-distributed temperature sensing to continuously quantify vertical flow in boreholes. *Water Resources Research*, *50*, 3706–3713. https://doi.org/10.1002/2014WR015273

Reiter, M. (2001). Using precision temperature logs to estimate horizontal and vertical groundwater flow components. *Water Resources Research*, *37*(3), 663–674. https://doi.org/10.1029/2000WR900302

Ren, T., Kluitenberg, G., & Horton, R. (2000). Determining soil mater flux and pore water velocity by a heat pulse technique. *Soil Science Society of America Journal*, *64*(2), 552. https://doi.org/10.2136/sssaj2000.642552x

Ren, T., Noborio, K., & Horton, R. (1999). Measuring soil water content, electrical conductivity, and thermal properties with a thermo-time domain reflectometry probe. *Soil Science Society of America Journal*, *63*(3), 450. https://doi.org/10.2136/sssaj1999.03615995006300030005x

Saar, M. O. (2011). Review: Geothermal heat as a tracer of large-scale groundwater flow and as a means to determine permeability fields. *Hydrogeology Journal*, *19*(1), 31–52. https://doi.org/10.1007/s10040-010-0657-2

Sayde, C., Thomas, C. K., Wagner, J., & Selker, J. (2015). High-resolution wind speed measurements using actively heated fiber optics. *Geophysical Research Letters*, *42*, 10,064–10,073. https://doi.org/10.1002/2015GL066729

Selker, F., & Selker, J. S. (2018). Investigating water movement within and near wells using active point heating and fiber optic distributed temperature sensing. *Sensors*, *18*(4), E1023.

Smith, L., & Chapman, D. S. (1983). On the thermal effects of groundwater flow: 1. Regional scale systems. *Journal of Geophysical Research*, *88*(B1), 593–608. https://doi.org/10.1029/JB088iB01p00593

Somogyvári, M., & Bayer, P. (2017). Field validation of thermal tracer tomography for reconstruction of aquifer heterogeneity. *Water Resources Research*, *53*, 5070–5084. https://doi.org/10.1002/2017WR020543

Stallman, R. W. (1965). Steady one-dimensional fluid flow in a semi-infinite porous medium with sinusoidal surface temperature. *Journal of Geophysical Research*, *70*(12), 2821–2827. https://doi.org/10.1029/JZ070i012p02821

Suzuki, S. (1960). Percolation measurements based on heat flow through soil with special reference to paddy fields. *Journal of Geophysical Research*, *65*(9), 2883–2885. https://doi.org/10.1029/JZ065i009p02883

Trainer, F. W. (1968). *Temperature profiles in water wells as indicators of bedrock fractures*. Reston: US Geological Survey professional paper.

Van Wielink, I. (2016). Karteren en modelleren van het zoet-brak grondwatersysteem in de Horstermeer (Master's thesis), Vrije Universiteit, Amsterdam.

Van de Giesen, N., Steele-Dunne, S. C., Jansen, J., Hoes, O., Hausner, M. B., Tyler, S., & Selker, J. (2012). Double-ended calibration of fiber-optic Raman spectra distributed temperature sensing data. *Sensors*, *12*(5), 5471–5485. https://doi.org/10.3390/s120505471

Vandenbohede, A., Louwyck, A., & Lebbe, L. (2009). Conservative solute versus heat transport in porous media during push-pull tests. *Transport in Porous Media*, *76*(2), 265–287. https://doi.org/10.1007/s11242-008-9246-4

Wagner, V., Bayer, P., Bisch, G., Kübert, M., & Blum, P. (2014). Hydraulic characterization of aquifers by thermal response testing: Validation by large-scale tank and field experiments. *Water Resources Research*, *50*, 71–85. https://doi.org/10.1002/2013WR013939

Wagner, V., Blum, P., Kübert, M., & Bayer, P. (2013). Analytical approach to groundwater-influenced thermal response tests of grouted borehole heat exchangers. *Geothermics*, *46*, 22–31. https://doi.org/10.1016/J.GEOTHERMICS.2012.10.005

Wilson, J. L., & Miller, P. J. (1978). Two-dimensional plume in uniform ground-water flow. *Journal of the Hydraulics Division*, *104*(4), 503–514.

Zheng, C., & Wang, P. P. (1999). MT3DMS: A modular three-dimensional multispecies transport model for simulation of advection, dispersion, and chemical reactions of contaminants in groundwater systems; documentation and user's guide (Tech. Rep.) Tuscaloosa, AL: Alabama University.

Zubair, S. M., & Chaudhry, M. A. (1996). Temperature solutions due to time-dependent moving-line-heat sources. *Heat and Mass Transfer*, *31*(3), 185–189. https://doi.org/10.1007/BF02333318